Layers of Distinct Mobility in Densely Grafted Dendrimer Arborescent Polymer Hybrids

Panagiotis Kardasis,[1] Nikolaos Kalafatakis,[2,3] Mario Gauthier,[4] Dimitris Vlassopoulos,[2,3] and George Floudas[1,5,*]

[1]Department of Physics, University of Ioannina, 45110 Ioannina, Greece
[2]Institute of Electronic Structure and Laser, Foundation for Research and Technology (FORTH), 70013 Heraklion, Crete, Greece
[3]Department of Materials Science & Technology, University of Crete, 70013 Heraklion, Crete, Greece
[4]Institute for Polymer Research, Department of Chemistry, University of Waterloo, Waterloo, Ontario N2L 3G1, Canada
[5]University Research Center of Ioannina (URCI)—Institute of Materials Science and Computing, 45110 Ioannina, Greece

(Received 14 February 2021; accepted 27 April 2021; published 21 May 2021)

Melts of multiarm stars of 1,4-polybutadiene (dendrimer arborescent hybrids) with very high branching functionality (f) and small arm molar mass behave as jammed colloids and show *distinct* layers of segmental mobility. Three mobility layers were identified, comprising outer, intermediate, and near-core segments, all displaying a Vogel-Fulcher-Tammann temperature dependence. The respective glass temperatures increase as $f^{1/2}$. Our findings pave the way for further progress in this field by reconsidering previous theoretical treatments based on a *single* friction coefficient in hybrid nanoparticles such as densely grafted stars.

DOI: 10.1103/PhysRevLett.126.207802

Long range motions in branched polymers are distinct from linear chains. In the simplest case of branched polymers, namely a star polymer composed of f linear chains grafted onto a small core, relaxation proceeds via arm retraction, a mechanism that depends on the arm length but not on functionality [1–9]. As f increases, another slower process reflects the cooperative rearrangement of the ordered stars [8–11]. In solution, the blob model of Daoud and Cotton [12] (f branches, N statistical units per branch of length l) identified three monomer density regimes: the outer (swollen) regime where excluded volume effects dominate within a blob, the intermediate (unswollen) regime where the density is high enough to screen the excluded volume interactions, and the inner or core regime where the density is highest, and presumably segments are not allowed to wiggle freely. In the limit of a very large number of branches, e.g., $f > N^2$, the whole star comprises a core of constant (high) density with radius $R \sim (Nf)^{1/3} l \sim Nl$, meaning that in this limit branches are stretched and the star exhibits particlelike behavior and rheological signatures of jamming [13–15]. In the majority of cases investigated so far [2–9,13,14,16,17], $f^{1/2} < N < f^2$, such that the highly stretched case of high branching density was not attained. In this limit star polymers behave as soft hybrids exhibiting liquidlike order, and both faster polymeric and slower colloidal viscoelastic responses [8–10,14,18,19].

Despite progress in understanding longtime dynamics, very little is known about the effect of dense star topology (in the limit $f \geq N^2$) on segmental dynamics with relevance in polymer processing [13,14,20–22]. To this end, recent models treating the linear viscoelastic response of multiarm star polymers assume a *single* friction coefficient associated with a single segmental relaxation [10]. Furthermore, controlling the range of segmental relaxations and the associated glass temperature variation is a prerequisite for versatile shape memory polymers [23]. Not surprisingly, in this endeavor, branched or star polymers have already been exploited in an effort to enhance the shape memory effect [24].

In this Letter, we employ dielectric spectroscopy and differential scanning calorimetry to explore the effect of the multiarm star topology on the segmental dynamics. The scientific question we address is *if* and *how* the crowded star topology affects the local segmental dynamics in multiarm star polymers that fulfil the condition $f \geq N^2$. This question has relevance in decoding the rheology and processing of soft composites and holds the key for the development of shape memory polymers. Results reveal that segments form three *distinct* layers of reduced mobility, from the periphery to the core. Notably, theoretical models of dynamics at larger length scales (e.g., arm retraction and slow colloidal processes) [10] need to consider multiple friction coefficients.

The molecular architecture and characteristics of the studied 1,4-polybutadiene dendrimer arborescent polymer hybrids are provided in Scheme SI and Table SI, Supplemental Material [25]. The sample nomenclature identifies the hydrosilylated starlike substrate (RS), the number (e.g., 64 or 128) of inner arms, and the target molar mass of the polybutadiene (PBD) outer arms (1.5 or 5 kg mol^{-1} as PBD1.5 and PBD5, respectively). Using the molar mass of a Kuhn monomer, $M_0 = 105\ g\,\mathrm{mol}^{-1}$ [1], we get for the three stars: $f > N^2$ (RS64-PBD1.5),

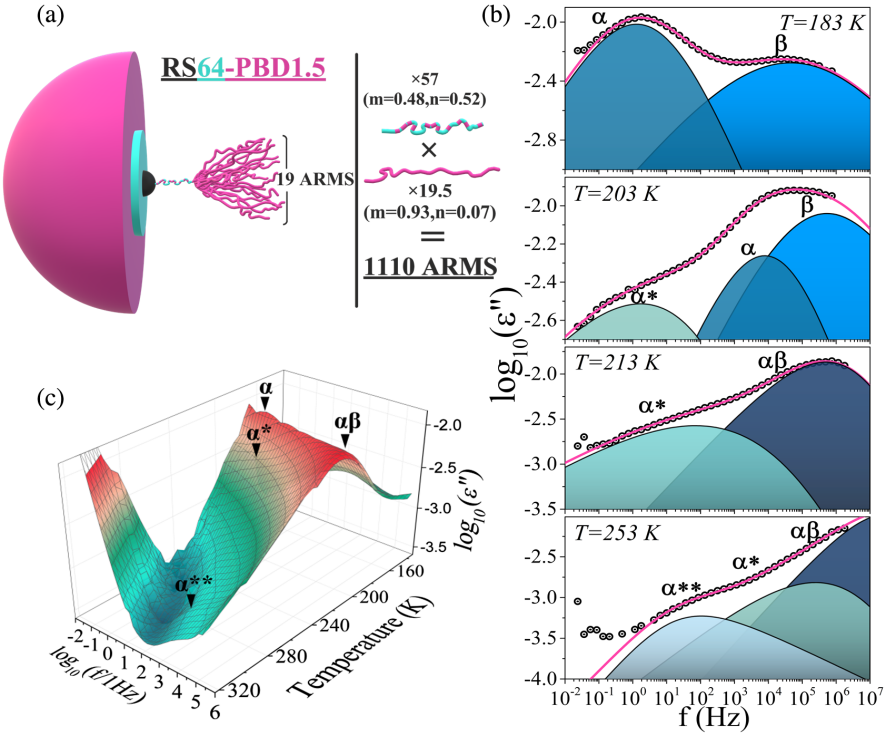

FIG. 1. (a) Schematic representation of the core-shell architecture of RS64-PBD1.5, assuming spherical symmetry. It consists of the carbosilane dendrimer core (black), the intermediate area (blue) composed of 57 PBD chains of mixed 1,4 (m) and 1,2 (n) microstructures, and the external region (pink) composed of 19.5 PBD chains (microstructure: $m = 0.93$, $n = 0.07$) per internal chain. (b) Dielectric loss curves as a function of frequency at selected temperatures; $T = 183$ K, $T = 203$ K, $T = 213$ K, and $T = 253$ K that better depict the β, α, merged $\alpha\beta$, α^*, and α^{**} processes. The red lines represent fits with a summation of Havriliak-Negami functions. Each process is represented with a different hue of blue color. (c) Three-dimensional representation of the dielectric loss curves of RS64-PBD1.5 as a function of temperature and frequency.

$f \gg N^2$ (RS128-PBD1.5), and $f \sim N^2$ (RS64-PBD5). Dielectric spectroscopy (DS) measurements were performed, in the range from 323–133 K for frequencies in the range from 10^{-2} to 10^7 Hz [31]. Differential scanning calorimetry (DSC) and temperature-modulated (TM DSC) measurements were made on a Q2000 (TA Instruments). A strain-controlled rheometer with a force rebalance transducer (ARES 2kFRTN1, from TA Instruments) was used for the rheology measurements. More details on the materials and methods can be found in the Supplemental Material [25].

Figure 1(a) provides a schematic representation of the core-shell architecture of RS64-PBD1.5. It depicts three regions consisting of the carbosilane dendrimer core, the intermediate area composed of 57 PBD chains of mixed microstructure [$m = 0.93$, $n = 0.07$], and the external region composed on average of 19.5 attached 1,4-PBD chains ($m = 0.93$, $n = 0.07$) per internal chain. This chemistry results in a very high branching functionality ($f = 1110$ PBD arms, in this case). Specific fitting examples with summations of Havriliak-Negami processes are provided in Fig. 1(b) at selected temperatures. Starting from lower temperatures the different processes reflect the local β relaxation, and to the segmental α, α^*, and α^{**} relaxations, corresponding to three distinct layers of mobility. The corresponding dielectric loss curves of RS64-PBD1.5 are shown in a 3D representation in Fig. 1(c). Details are provided in the Supplemental Material (Figs. S1–S9) [25].

Informative with respect to the effect of increasing branching functionality on the segmental dynamics is the comparison of the dielectric loss curves (for the different samples) with linear PBD at the same reference temperature. Superimposed dielectric loss curves are compared in Fig. 2 around the maximum corresponding to the α relaxation as $b_T\varepsilon''$ ($\alpha_T f$; T_{ref}), where α_T is a single frequency-scale shift factor and b_T is a small single loss-scale shift factor at a temperature T. Slower processes contribute to the dielectric loss in the arborescent hybrids, in contrast to the single α relaxation of the PBD homopolymer. Evidently, with increasing functionality, the α relaxation shifts to lower frequencies and its dielectric strength is reduced at the expense of the slower processes. In the case of RS128-PBD1.5, with the highest functionality ($f = 2830$), the slower processes (corresponding to the α^* and α^{**} relaxations) gain more intensity than the α relaxation. The analysis is supported by a model free evaluation of the distribution of relaxation times [Figs. 2(b) and 2(c)] (based on the Tikhonov algorithm, Supplemental Material [25]).

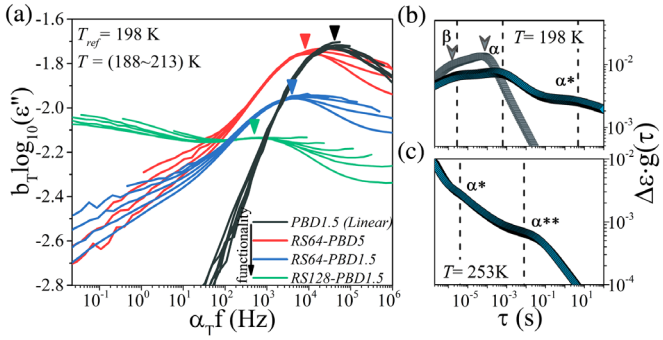

FIG. 2. (a) Comparison of superimposed dielectric loss curves for RS128-PBD1.5 (green lines), RS64-PBD1.5 (blue lines), RS64-PBD5 (red lines), and PBD1.5 homopolymer (black lines) at a reference temperature of 198 K. The curves have been shifted horizontally and vertically by their respective shift factors, α_T and b_T. The vertical arrows indicate the maximum loss corresponding to the α relaxation. (b),(c) Distribution of relaxation times extracted by a generalized regularization method for the homopolymer PBD1.5 (gray squares) and RS64-PBD1.5 (blue rhombi) at selected temperatures. The arrows and vertical lines indicate the corresponding relaxation times for the homopolymer and the hybrid.

The temperature dependence of the different relaxation processes can be discussed with the help of Fig. 3. The figure compares the characteristic frequencies at maximum loss for linear 1,4-PBD [32] with the 1,4-PBD in the arborescent hybrids, all with a similar arm molar mass, as a function of increasing number of arms. It depicts a fast β relaxation with an Arrhenius temperature dependence, $f_{\max} = f_0 \exp(-(E/RT))$, where $f_{\max}$ is the frequency at maximum loss, f_0 the limiting frequency at very high temperatures, and E is the apparent activation energy (32.0 ± 0.5 kJ mol^{-1}) that is unaffected by functionality. At higher T, the α relaxation exhibits a Vogel-Fulcher-Tammann (VFT) temperature dependence according to $f_{\max} = f_0 \exp(-(B/T - T_0))$, where B is the activation parameter and T_0 is the "ideal" glass temperature. The corresponding glass temperature T_g is associated with freezing of the segmental dynamics, together with the VFT parameters provided in Table I. Two slower processes are evident in RS64-PBD1.5 corresponding to the α^* and α^{**} relaxations, also with a VFT temperature dependence.

The presence of multiple segmental dynamics within a single polymer is possible [33]—albeit not common—and depends on the particular polymer topology and the sensitivity of the probing technique. The origin of the three distinct processes with the VFT T dependence is discussed with the help of results from DS (Fig. 3 and Figs. S1–S9), DSC (Figs. S10, S11) and rheology (Figs. S12, shown in the Supplemental Material [25]). In RS64-PBD1.5 the α relaxation (with respective low- and high-frequency slopes of 0.43 ± 0.05 and 0.56 ± 0.05) has an effective dielectric strength of $T\Delta\varepsilon = 6 \pm 2$ K. The α^* relaxation (low- and high-frequency slopes of 0.35 ± 0.08 and 0.56 ± 0.05, respectively) has $T\Delta\varepsilon = 4.5 \pm 1$ K, whereas for the α^{**} relaxation $T\Delta\varepsilon = 1.2 \pm 0.3$ K. Concomitantly, TM-DSC (Fig. S10) exhibits two steps in the specific heat at temperatures that correspond to the DS α and α^* relaxations. In addition, a careful examination of the linear viscoelastic master curves (phase angle as a function of complex modulus, van Gurp-Palmen plot, Fig. S12) reveals the breakdown of time-temperature superposition in the vicinity of T_g.

These results, taken together, suggest the following origin of the three processes. The α relaxation is assigned to freezing of the dynamics of the outer 1,4-PBD segments of the arborescent hybrids (characteristic correlation length ~2.7 nm, Table II). This relaxation bears similarities with the α relaxation of linear PBD. However, it shows an increased glass temperature by as much as ~11 K which depends on functionality (Fig. 4), as well as an increased fragility index (m from 65 in linear PBD to ~80 in the arborescent hybrids, Table II). This implies that even the segmental dynamics of the outer PBD segments are affected by the highly branched topology. The α^* relaxation is assigned to the freezing of the dynamics of an intermediate layer (characteristic correlation length ~1.4 nm). The corresponding freezing temperature is also a strong function of branching functionality, increasing by up to ~34 K relatively to linear PBD. Last, the α^{**} relaxation is assigned to the dynamics of those PBD segments in the vicinity of the core. At the star core crowding of the chains precludes wiggling motions, leading to a much slower segmental relaxation. Within the timescale of the α^{**} relaxation, some contribution from 1,2-PBD segments is expected [approximately a third of the effective dielectric strength and the fraction (~5%) of 1,2-PBD segments] [34]. Evidently, the correlation lengths of the outer and intermediate layers comprise about half the star size in

TABLE I. Parameters of the Vogel-Fulcher-Tammann equation for the α, α^*, and α^{**} relaxation of 1,4-polybutadiene arborescent hybrids. (# represents value held constant.).

	α relaxation				α^* relaxation				
SAMPLE	$\log f_0$	B (K)	T_0 (K)	T_g (K)	$\log f_0$	B (K)	T_0 (K)	RS64-PBD1.5	α^{**} relaxation
RS64-PBD1.5	12#	1043 ± 34	146 ± 1	179 ± 1	12#	1806 ± 30	136 ± 1	$\log f_0$	7.0 ± 0.3
RS64-PBD5	12#	1010 ± 36	145 ± 1	176 ± 1	12#	1751 ± 30	130 ± 1	B (K)	988 ± 150
RS128-PBD1.5	12#	891 ± 31	154 ± 1	183 ± 1	12#	1755 ± 42	153 ± 2	T_0 (K)	165 ± 7

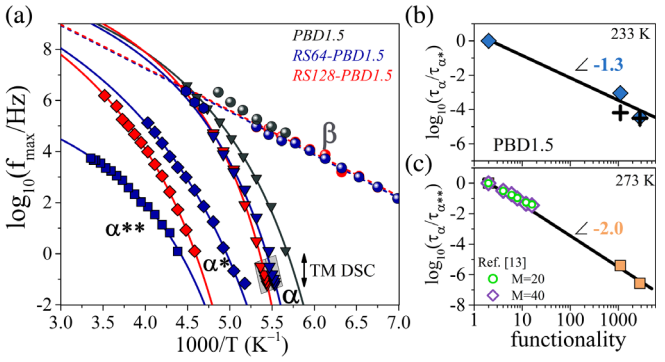

FIG. 3. (a) Arrhenius relaxation map for a series of 1,4-PBD arborescent hybrids with a similar arm molecular weight but increasing number of arms: segmental α relaxation (down triangles), local β relaxation (circles), α^* relaxation (rhombi) for different functionalities: RS128-PBD1.5 (red), RS64-PBD1.5 (blue), and PBD1.5 (black). A slower α^{**} relaxation (squares) is evident in RS64-PBD1.5. Data inside the gray box were obtained from TM DSC. The curved and the straight lines represent fits to the VFT and the Arrhenius equations, respectively. (b),(c) Structural relaxation time ratios, $(\tau_\alpha/\tau_{\alpha^*})$ and $(\tau_\alpha/\tau_{\alpha^{**}})$, as a function of functionality. Simulation data for different numbers of repeating units M are included from Ref. [13]. Crosses in (b) are from rheology (arm retraction mechanism [15] and Supplemental Material, Figs. S12 and S13 [25]).

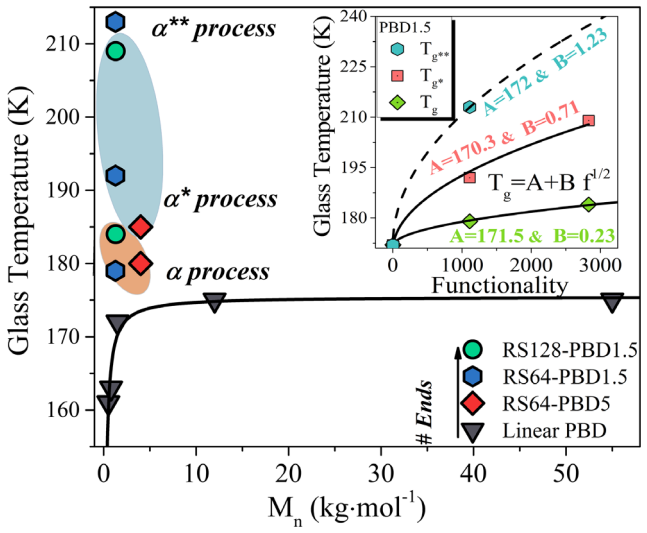

FIG. 4. Glass temperatures ($\tau = 100$ s) as a function of molecular mass for RS128-PBD1.5 (green circles), RS64-PBD1.5 (blue hexagons), RS64-PBD5 (red rhombi), and PBD1.5 (black down triangles). The black line is a fit to the Fox-Flory equation. The inset gives the glass temperatures (obtained from DS) as a function of functionality for the hybrids with a molecular mass of $M_n = 1.3$ kg mol^{-1}. The lines are fits to a square root dependence of functionality (see also Fig. S14).

RS64-PBD5 [11] (Table II) and correspond to the interpenetration regime in the two-layer model of polymer-grafted nanoparticles [11].

The disparate dynamics of the *outer*, *intermediate*, and *near-core* PBD segments can be discussed with the help of Figs. 3(b) and 3(c) as a function of functionality. In Fig. 3(b) the magnitude of the difference of the outer and intermediate dynamic layers, $\tau_\alpha/\tau_{\alpha*}$, has a power law dependence on functionality as $f^{-1.3}$. Additional data from rheology, corresponding to the arm relaxation mechanism, are included in the figure [15]. We need to comment, however, that DS is not sensitive to large scale motions, as PBD does not have a dipole along the chain. The apparent agreement of the timescale for the segmental α^* relaxation with the arm relaxation found in rheology can be explained as follows: as the PBD arm undergoes a slow and hindered retraction mechanism, segments are displaced from the star periphery to the intermediate layer—as the approach to the core is prohibited—thus contributing to the dielectrically active α^* relaxation. For the α^{**} relaxation the difference in the outer and core dynamic layers $\tau_\alpha/\tau_{\alpha**}$ exhibit another power law dependence as $f^{-2.0}$. In the same plot, simulation data from star polymer melts with a much lower functionality are included corresponding to the near-core segments [13] with a dependence on functionality as $f^{-1.63}$. Overall, the results of Figs. 3(b) and 3(c) demonstrate that functionality enhances the intramolecular dynamic heterogeneity.

The results for the freezing of the different relaxation processes (α, α^*, and α^{**} processes at $\tau = 100$ s) can be discussed with respect to the respective glass temperatures in Fig. 4. In the RS64-PBD1.5 arborescent hybrid the α relaxation is located some 4 K higher (179 K), and the two (α^* and α^{**}) processes now freeze at 192 and 213 K, respectively. The effect of functionality is shown in the inset. In general, the different glass temperatures follow a $f^{1/2}$ dependence, in qualitative agreement with the results from a recent simulation [14].

The experimental results are compared with simulations in lower functionality stars [13,14], which identified a mobility *gradient* of relaxation as a function of the distance from the star core. From the heterogeneous dynamics only two kind of segments were considered, located at the end of the star and near the core. Herein, instead, we identified three distinct layers of mobility and show that intermediate and core segments have *different* power law dependencies on functionality ($f^{-1.3}$ and $f^{-2.0}$, respectively). Of relevance to the current work is an NMR study on a 4-arm polybutadiene star, having sequences with molar mass comprising an entanglement strand and situated at various distances from the free end of the star arm down to the core [20]. Three distinct deuterium transverse relaxation times T_2 were found corresponding to the various labeled segments of the star arm (periphery, core, and intermediate sections). However, with a single star no predictions could be made on the effect of functionality. In the present case, with f in excess of 900, these timescales can be very well separated without the need for labeling which, inevitably, introduces some thermodynamic issues.

TABLE II. Characteristic parameters of 1,4-polybutadiene arborescent hybrids.

Sample (kg mol^{-1})	f	T_g (K)	C_{1g} [a]	C_{2g}(K)[a]	m [b]	T_{g*} (K) [c]	$T_{g^{**}}$ (K) [c]	ξ_α (nm) [d]	R (nm)
PBD1.5	2	172	13.2	35	65.9	⋯	⋯	2.1	1.48 [f]
RS64-PBD5	929	176	14.2	31	80.3	185	⋯	2.7	12.2 [e]
RS64-PBD1.5	1110	179	13.7	33	74.5	192	213	2.8	8.8 [e]
RS128-PBD1.5	2830	183	14.7	29	84.2	209 (DS)			
						203 (DSC)	⋯	2.3	12.2 [e]

[a]WLF parameters calculated at the glass temperature of the α relaxation.
[b]Fragility [$m = BT_g/2.303(T_g - T_0)^2$].
[c]Expected freezing temperature (defined at $\tau = 100$ s) of α^* and α^{**} relaxations.
[d]Correlation length of α relaxation obtained from the step in heat capacity as $\xi_\alpha = (k_B T_g^2 \Delta(1/c_p)/\rho(\delta T)^2)^{1/3}$ and $\Delta(1/c_p) = (1/c_p^{\text{glass}}) - (1/c_p^{\text{liquid}})$ (see Fig. S10).
[e]Star size estimated as [11] $R = \sqrt[3]{(R_c^3 + (3fN_{\text{arm}}/4\pi)(M_0/\rho_{\text{mass}}N_A))}$, where R_c is the inorganic core (estimated as 2.29 and 2.72 nm in RS64 and RS128, respectively), and the radius of gyration of intermediate PBD (1.21 nm), $M_0 = 105\ g\,\text{mol}^{-1}$ [1], and ρ_{mass} is the mass density ($0.826\ g\,\text{cm}^{-3}$) [1].
[f]Radius of gyration calculated from $\langle R_o^2\rangle/M = 0.876$ (Å^2) as $\langle R_g^2\rangle = \langle R_o^2\rangle/6M$ [35].

The results can also be compared with segmental relaxation in polymer nanocomposites based on polymer-grafted nanoparticles [36–39]. In that case, the inorganic cores constitute a substantial part of the composite (typically around 40 vol/vol%). In general, they exhibit a higher T_g than the bulk and a broad distribution of relaxation times. In certain cases [36,37], the distribution could be decomposed into "interfacial" and "average" segmental relaxations. However, there exist some differences with the present hybrids. First, the inorganic core in the hybrids is in a range from 0.6 to 1.8 vol/vol%. Second, the grafting density in the present hybrids is much higher (6 to 15 chains/nm^2, as compared to ~0.3 chains/nm^2 in the composites) making the chains highly stretched, giving rise to distinct segmental dynamics in the outer and intermediate layers.

In conclusion, it was found that a series of multiarm stars of 1,4-polybutadiene melts of extremely high branching functionality behave as jammed soft colloids with distinct layers of segmental mobility. Three mobility layers were identified, comprising outer, intermediate, and near-core PBD segments, all with a VFT temperature dependence. Notably, functionality affected even the dynamics of those segments located in the outer layer, that showed slower dynamics and higher fragility. The magnitude of the difference in relaxation times of the outer with the intermediate and the core PBD segments displayed power law dependences on functionality (as $f^{-1.3}$ and $f^{-2.0}$, respectively). Additionally, the corresponding glass temperatures display a $f^{1/2}$ dependence. These results demonstrate unanticipated rich dynamics of the hybrids, both at long (arm and star relaxation) and short timescales (segmental relaxation). They pave the way for further progress in this field by accounting for multiple friction coefficients in polymer hybrids.

This study demonstrated unambiguously and quantitatively how a branched topology affects segmental dynamics. Specifically, solvent-free star-shaped jammed colloids exhibit a low-frequency colloidal plateau, but at the same time also display distinct segmental dynamics, with associated T_g's that are much higher than in the corresponding linear chains. As similar results are to be expected for other highly branched topologies, the results reported herein need to be considered during composite processing by adjusting the temperature. Additionally, the induced dynamic heterogeneity at the segmental level is beneficial in the design of soft composites based on amorphous shape memory polymers.

This research was supported by the Hellenic Foundation for Research and Innovation (H. F. R. I.) under the "First Call for H. F. R. I. Research Projects to support Faculty members and Researchers and the procurement of high-cost research equipment grant" (Project No. 183) and the Hellenic Department of Development under the "Research-Creation-Innovation" initiative (project PANHYDROMED).

*Corresponding author.
gfloudas@uoi.gr

[1] M. Rubinstein and R. H. Colby, *Polymer Physics* (Oxford University Press, New York, 2003).
[2] S. T. Milner and T. C. B. McLeish, Macromolecules **30**, 2159 (1997).
[3] C. H. Adams, L. R. Hutchings, P. G. Klein, T. C. B. McLeish, and R. W. Richards, Macromolecules **29**, 5717 (1996).
[4] J. Roovers, Polymer **26**, 1091 (1985).
[5] L. Fetters, A. D. Kiss, D. S. Pearson, G. F. Quack, and F. J. Vitus, Macromolecules **26**, 647 (1993).
[6] X. Qiao, T. Sawada, Y. Matsumiya, and H. Watanabe, Macromolecules **39**, 7333 (2006).
[7] Y. Matsumiya, Y. Masubuchi, T. Inoue, O. Urakawa, C.-Y. Liu, E. van Ruymbeke, and H. Watanabe, Macromolecules **47**, 7637 (2014).
[8] T. Pakula, Comput. Theor. Polym. Sci. **8**, 21 (1998).

[9] D. Vlassopoulos, T. Pakula, G. Fytas, J. Roovers, K. Karatasos, and N. Hadjichristidis, Europhys. Lett. **39**, 617 (1997).
[10] M. Kapnistos, A. N. Semenov, D. Vlassopoulos, and J. Roovers, J. Chem. Phys. **111**, 1753 (1999).
[11] J. Midya, M. Rubinstein, A. K. Kumar, and A. Nikoubashman, ACS Nano **14**, 15505 (2020).
[12] M. Daoud and J. P. Cotton, J. Phys. **43**, 531 (1982).
[13] A. Chremos, E. Glynos, and P. F. Green, J. Chem. Phys. **142**, 044901 (2015).
[14] J. Fan, H. Emamy, A. Chremos, J. F. Douglas, and F. W. Starr, J. Chem. Phys. **152**, 054904 (2020).
[15] L. Gury, M. Gauthier, M. Cloitre, and D. Vlassopoulos, Macromolecules **52**, 4617 (2019).
[16] D. Boese, F. Kremer, and L. J. Fetters, Macromolecules **23**, 1826 (1990).
[17] K. L. Ngai and C. M. Roland, J. Polym. Sci., Polym. Phys. **35**, 2503 (1997).
[18] C. N. Likos, Phys. Rep. **348**, 267 (2001).
[19] C. N. Likos, H. Löwen, M. Watzlawek, B. Abbas, O. Jucknischke, J. Allgaier, and D. Richter, Phys. Rev. Lett. **80**, 4450 (1998).
[20] C. H. Adams, M. G. Brereton, L. R. Hutchings, P. G. Klein, T. C. B. McLeish, R. W. Richards, and M. E. Ries, Macromolecules **33**, 7101 (2000).
[21] F. Rietsch, D. Daverloose, and D. Froelich, Polymer **17**, 859 (1976).
[22] C. Mayer, F. Sciortino, C. N. Likos, P. Tartaglia, H. Löwen, and E. Zaccarelli, Macromolecules **42**, 423 (2009).
[23] T. Xie, Nature (London) **464**, 267 (2010).
[24] M. Bothe, K. Y. Mya, E. M. J. Lin, C. C. Yeo, X. Lu, C. He, and T. Pretsch, Soft Matter **8**, 965 (2012).
[25] See Supplemental Material at http://link.aps.org/supplemental/10.1103/PhysRevLett.126.207802 for further details on the synthesis, DS data evaluation, DSC, and rheology, which includes Refs. [26–30].
[26] M. Gauthier and A. Munam, Macromolecules **43**, 3672 (2010).
[27] T. Roths, M. Marth, J. Weese, and J. Honerkamp, Comput. Phys. Commun. **139**, 279 (2001).
[28] J. Grebowicz, W. Aycock, and B. Wunderlich, Polymer **27**, 575 (1986).
[29] O. Laukkanen, Rheol. Acta **56**, 661 (2017).
[30] P. Zoller and D. J. Walsh. *Standard Pressure-Volume-Temperature Data for Polymers* (Technomic Publ. Co., 1995).
[31] F. Kremer and A. Schönhals, *Broadband Dielectric Spectroscopy* (Springer, Berlin, 2002).
[32] S. Alexandris, P. Papadopoulos, G. Sakellariou, M. Steinhart, H.-J. Butt, and G. Floudas, Macromolecules **49**, 7400 (2016).
[33] A. Pipertzis, A. Hess, P. Weis, G. Papamokos, K. Koynov, S. Wu, and G. Floudas, ACS Macro Lett. **7**, 11 (2018).
[34] C. M. Roland, R. Casalini, P. Santangelo, M. Sekula, J. Ziolo, and M. Paluch, Macromolecules **36**, 4954 (2003).
[35] L. J. Fetters, D. J. Lohse, D. Richter, T. A. Witten, and A. Zirkel, Macromolecules **27**, 4639 (1994).
[36] A. P. Holt *et al.* ACS Nano **10**, 6843 (2016).
[37] I. Popov, B. Carroll, V. Bocharova, A.-C. Genix, S. Cheng, A. Khamzin, A. Kisliuk, and A. P. Sokolov, Macromolecules **53**, 4126 (2020).
[38] X. Liu, N. W. Utomo, Q. Zhao, J. Zheng, D. Zhang, and L. A. Archer, Macromolecules **54**, 426 (2021).
[39] N. Sakib, Y. P. Koh, Y. Huang, K. I. S. Mongcopa, A. N. Le, B. C. Benicewicz, R. Krishnamootri, and S. K. Simon, Macromolecules **53**, 2123 (2020).